Palaeogeography, Palaeoclimatology, Palaeoecology 465 (2017) 237–246

Contents lists available at ScienceDirect

Palaeogeography, Palaeoclimatology, Palaeoecology

journal homepage: www.elsevier.com/locate/palaeo

Constraining paleohydrologic change during the Paleocene-Eocene Thermal Maximum in the continental interior of North America

Allison A. Baczynski [a,*], Francesca A. McInerney [a,1], Scott L. Wing [b], Mary J. Kraus [c], Jonathan I. Bloch [d], Ross Secord [d,2]

[a] Department of Earth and Planetary Sciences, Northwestern University, Evanston, IL 60208, USA
[b] Department of Paleobiology, NHB121, PO Box 37012, Smithsonian Institution, Washington, D.C. 20013-7012, USA
[c] Department of Geological Sciences, University of Colorado Boulder, Boulder, CO 80309, USA
[d] Florida Museum of Natural History, University of Florida, Gainesville, FL 32611, USA

ARTICLE INFO

Article history:
Received 8 March 2016
Received in revised form 2 October 2016
Accepted 21 October 2016
Available online 23 October 2016

Keywords:
Paleocene-Eocene
PETM
n-Alkanes
Hydrogen isotopes
Paleohydrology
Apparent fractionation

ABSTRACT

Quantifying the relationship between carbon cycle perturbations and the hydrologic cycle in the geologic past is crucial to accurately modeling how future anthropogenic carbon emissions and resulting radiative forcing might affect the hydrologic cycle. Interpreting changes in proxy records for insight into paleohydrologic change is complex, and documented records of paleohydrologic response to past global warming are rare. We use the relationship between two independent proxy records, the stable isotope ratios of hydrogen in *n*-alkanes and oxygen in tooth enamel of *Coryphodon*, to examine paleohydrologic change in the continental interior of North America during the Paleocene-Eocene Thermal Maximum (PETM) hyperthermal ~56 Ma. The *Coryphodon* $\delta^{18}O$ record allows us to infer shifts in surface water isotope values through time by applying an empirical relationship between tooth enamel and precipitation $\delta^{18}O$ values. Precipitation $\delta^{18}O$ values increase by ~4‰ during the PETM, but *n*-alkane hydrogen isotope ratios show no directional change during the PETM. We explore multiple hypotheses that could explain the differences between the isotope records, including a change in apparent fractionation as a result of plant community change, a shift in the slope of the local meteoric water line, a change in the season of rainfall, or a shift in the season of lipid production. We model the changes that would be required to reconcile the isotope records for each hypothesis and evaluate the likelihood of each of the scenarios. We posit that the most likely hypothesis for the observed differences between the isotope records is a change in either the season of rainfall or the season of lipid production during the PETM.

1. Introduction

One of the important uncertainties in climate change projections is how the hydrologic cycle might respond to increasing pCO_2 and temperature. Although climate models are improving in their characterization of precipitation patterns at a global scale, there remains a significant amount of uncertainty at the regional scale (Collins et al., 2013), particularly for the interior of continents (Solomon et al., 2009). Theoretical calculations and global climate models predict that positive radiative forcing from rising pCO_2 levels will increase the prevalence of extreme precipitation events and that both floods and droughts will vary both spatially and temporally (Collins et al., 2013).

The concentration of carbon dioxide in the atmosphere affects global climate not only due to radiative forcing, but also by its influence on plant physiology. Plants regulate the opening and closing of stomata, pores on the surface of the leaf, based on environmental conditions including temperature, humidity, and availability of carbon dioxide. When carbon dioxide concentrations are high, stomata open less and transpiration decreases. The reduction in moisture flux from Earth's surface to the atmosphere results in higher temperatures near the surface (Betts et al., 2007; Ciais et al., 2013). While it is unknown exactly how much physiological forcing will contribute to overall climate change, recent studies have suggested that the indirect physiological forcing of plants will have a greater influence on global temperature than the direct radiative effects of carbon dioxide (Cao et al., 2010). Characterizing hydrologic change in the geologic past will expand our understanding of how Earth's climate and ecosystems respond to perturbations of the

* Corresponding author at: Department of Geosciences, Pennsylvania State University, Deike Building, University Park, PA 16802, USA.
E-mail address: aab27@psu.edu (A.A. Baczynski).
[1] Current address: Department of Earth Sciences and Sprigg Geobiology Centre, University of Adelaide, Adelaide, SA, Australia.
[2] Current address: Department of Earth and Atmospheric Sciences, University of Nebraska, Lincoln, NE 68588, USA.

http://dx.doi.org/10.1016/j.palaeo.2016.10.030
0031-0182/

carbon cycle and associated global warming and is key to understanding how future anthropogenic carbon emissions may influence the hydrologic cycle.

One of the largest and most rapid natural perturbations to the global carbon cycle occurred ~56 Ma at the Paleocene-Eocene boundary. This event, known as the Paleocene-Eocene Thermal Maximum (PETM), was an abrupt (≤20,000 years), transient (<200,000 years) episode of extreme (~5 to 8 °C) global warming that is recognized as the warmest period of the Cenozoic Era (Kennett and Stott, 1991; McInerney and Wing, 2011; Sluijs et al., 2007; Zachos et al., 1993; Zachos et al., 2001). The late Paleocene through early Eocene has long been recognized as a period of biotic change, which has been primarily attributed to rapid temperature change and increased pCO_2. However, associated changes in the hydrologic cycle, such as the amount and/or seasonality of precipitation, may have been a key driver of the observed terrestrial ecosystem changes.

The degree to which precipitation patterns were altered during the PETM is poorly understood, with interpretations of hydrologic proxies from sites across the globe ranging from considerably wetter conditions to significantly drier conditions and everything in between. An increase in the abundance of kaolinite and terrestrial palynomorphs along the northeastern margin of the United States, and in New Zealand and Antarctica, have been cited as evidence for enhanced erosion and runoff, which in turn have been attributed to increased precipitation and wetter PETM conditions (Cramer et al., 1999; Crouch et al., 2003; Gibson et al., 2000; Kaiho et al., 1996; Robert and Kennett, 1994). Some general circulation models and models of carbon cycling processes have suggested higher relative humidity in continental interiors during the PETM (Bowen et al., 2004; Huber and Sloan, 1999). Yet other studies have suggested regional variations, with greater relative humidity at higher latitudes and more arid conditions at subtropical latitudes (Bowen and Bowen, 2008; Pagani et al., 2006; Wing et al., 2005). Previous paleobotanical, paleopedologic, and isotopic studies from the PETM in the southeastern Bighorn Basin, WY, have indicated that the continental interior of North America may have experienced alternating episodes of wet and dry conditions during the PETM (Kraus et al., 2013; Kraus and Riggins, 2007; Secord et al., 2012; Smith et al., 2007; Wing et al., 2005). Additionally, Schmitz and Pujalte (2003, 2007) have proposed generally arid PETM conditions, but with an increase in seasonally extreme precipitation in mid-latitude continental Spain. Changes in fluvial deposition in western Colorado also suggest that flooding was common during the PETM and may indicate greater variability in the intensity of rainfall events (Foreman et al., 2012). More data are required to evaluate whether such differing interpretations reflect real spatial variations in precipitation, different sensitivities or seasonal biases of the individual proxies, or possibly misinterpretation of some paleohydrologic proxy data.

n-Alkanes are frequently used as a paleoclimate proxy because of their high preservation potential and resistance to isotopic exchange (Pedentchouk et al., 2006; Schimmelmann et al., 2006; Sessions et al., 2004). High molecular weight *n*-alkanes with a marked predominance of odd-over-even carbon chain lengths (C_{25} to C_{35}) are important constituents of the epicuticular waxes of vascular plants (Eglinton and Hamilton, 1967) and can serve as indicators of terrestrial plant input. The hydrogen incorporated into *n*-alkanes originates from meteoric water, which is influenced by temperature, humidity, evaporation, rainfall amount and water vapor source (Craig, 1961; Craig and Gordon, 1965; Gat, 1996; Rozanski et al., 1993). Because modern *n*-alkane hydrogen isotope (δD) ratios are highly correlated with the hydrogen isotopic signature of meteoric water at the time of their biosynthesis (Kahmen et al., 2011; Sachse et al., 2010; Sachse et al., 2009; Tipple et al., 2013), shifts in δD ratios of *n*-alkanes from geologic records are often equated to shifts in paleoclimate.

The *n*-alkane δD records from the Bighorn Basin, Lomonosov Ridge in the Arctic Ocean, and Tanzania suggest a positive shift in δD values at the onset of the PETM, which has been offered as evidence for drier conditions in mid-latitudes and increased moisture transport to the Arctic (Handley et al., 2008; Pagani et al., 2006; Smith et al., 2007). Conversely, records from Italy, France, New Zealand and Columbia/Venezuela suggest a negative shift in δD values at the onset of the PETM (Garel et al., 2013; Handley et al., 2011; Jaramillo et al., 2010; Krishnan et al., 2015; Tipple et al., 2011). The negative shift in δD values has been interpreted as indicating a wetter or more humid climate state at some sites (Garel et al., 2013; Handley et al., 2011). Additionally, the shift to more positive δD values prior to the onset of the CIE in some records suggests there may have been significant changes in the hydrologic cycle prior to the PETM (Garel et al., 2013; Tipple et al., 2011).

Interpreting changes in paleohydrology using *n*-alkane δD records is challenging because the isotope ratios of modern plant lipids reflect not only the δD ratio of meteoric water but also the D-enrichment of leaf water resulting from evaporation and/or transpiration and isotopic fractionation that occurs during *n*-alkane biosynthesis (Kahmen et al., 2013a; Kahmen et al., 2013b; Sachse et al., 2012; Sachse et al., 2006; Smith and Freeman, 2006). This makes it extremely difficult, if not impossible, to interpret climate regime based solely on shifts in lipid δD values. Furthermore, the high molecular concentrations required for *n*-alkane δD analysis restrict the number of measurements that can be made, and the few PETM *n*-alkane δD records that do exist commonly have a much lower resolution than the corresponding *n*-alkane carbon isotope ($\delta^{13}C$) curves.

Previous studies have not been able to independently examine changes in plant community composition and the isotope ratios of precipitation, both of which contribute to the *n*-alkane δD signature. In this study, we measure the hydrogen isotope values of *n*-alkanes and explicitly characterize these effects. Specifically, we consider how the shift from a mixed angiosperm/conifer to predominantly angiosperm flora and the increase in proportion of monocots (Smith et al., 2007; Wing and Currano, 2013; Wing et al., 2005) would affect apparent fractionation between source water and leaf wax lipids. We also independently constrain changes in the isotopic composition of precipitation by applying an empirically derived relationship between tooth enamel and precipitation oxygen isotope ($\delta^{18}O$) values to *Coryphodon* tooth enamel $\delta^{18}O$ values (Kohn and Dettman, 2007). The $\delta^{18}O$ and δD isotope profiles differ, suggesting that the *n*-alkane record does not directly record changes in annual precipitation isotope ratios. We explore several explanations for reconciling the isotope records by modeling changes in the local meteoric water line, seasonality of precipitation, and apparent fractionation, and assess the likelihood of each scenario. The ability to independently constrain precipitation isotope values and changes in plant community allows a unique exploration of paleohydrologic change during the PETM.

2. Methods

2.1. Study area and sample collection

The Bighorn Basin, WY (Fig. 1) preserves an unusually complete and expanded continental stratigraphic record of the early Paleogene (Bown, 1980; Wing, 1998). Extensive sedimentological, geochemical, and paleontological research has established a strong lithostratigraphic, biostratigraphic, and chemostratigraphic framework for the PETM in the southeastern Bighorn Basin (see Baczynski et al., 2013). Bulk organic carbon, *n*-alkane, and mammalian tooth enamel carbon isotope records from the southeastern Bighorn Basin, WY independently document the negative carbon isotope excursion (CIE) associated with the PETM. A shift to more negative carbon isotope values marking the onset of the PETM is corroborated by biostratigraphic data, with the first appearances of earliest Eocene (Wa-0) mammals. Likewise, the carbon isotope recovery in *n*-alkanes and tooth enamel is coincident with a change in floral composition and a faunal shift from biozone Wa-0 to Wa-1 (Baczynski et al., 2013; Baczynski et al., 2016; Secord et al., 2012). The

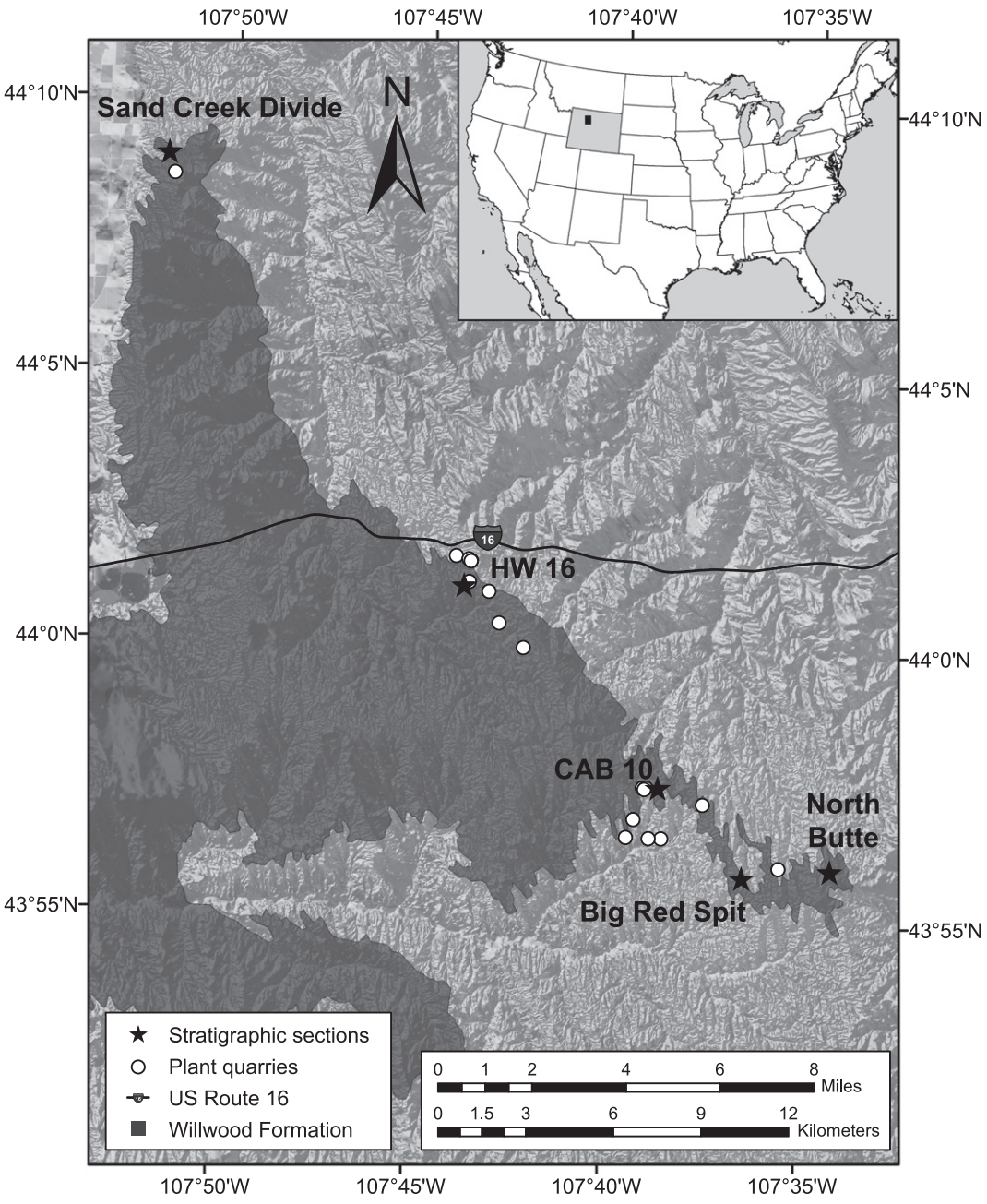

Fig. 1. Map of field area in the southeastern Bighorn Basin, Wyoming showing exposures of the Willwood Formation (shaded). Stars designate locations of detailed PETM stratigraphic sections at HW 16, CAB 10, Big Red Spit, and North Butte (see Baczynski et al., 2013). Circles mark locations of floral localities for which *n*-alkane δD values were measured. Map scale is 1:140,000.

PETM interval, as defined by biostratigraphy and compound specific stable carbon isotopes, is indicated by gray shading in all figures (Fig. 2A).

The PETM corresponds with the transition from the Fort Union Formation to the Willwood Formation in the southeastern Bighorn Basin (Kraus et al., 2013; Rose et al., 2012; Secord et al., 2012; Wing et al., 2009). These formations are comprised of mudstones, fine-grained sandstones, and carbonaceous shales that were deposited by small fluvial systems in floodplain, channel or channel margin, and swamp-like environments (Baczynski et al., 2013; Kraus et al., 2013; Wing, 1998; Wing et al., 2005). Organic-rich rock samples were collected from isolated lenticular channel fills (~3–5 m thick and <50 m across) where plant macrofossils were found (Baczynski et al., 2013; Baczynski et al., 2016; Wing and Currano, 2013; Wing et al., 2005). Surface material was removed from the plant-bearing beds to expose well-consolidated rock. Organic-rich rock samples for *n*-alkane analysis were collected using a rock hammer and placed in cloth bags for transport and storage. Thirty-six rock samples for *n*-alkane δD analysis were collected from twenty-eight unique stratigraphic levels, spanning roughly 100 m of Paleocene-Eocene section in the southeastern Bighorn Basin, Wyoming. GPS coordinates were recorded at each site. From their position within local stratigraphic sections, *n*-alkane sites were projected onto a single interpolated composite curve (Baczynski et al., 2016).

2.2. Lipid extraction and separation

The exterior of each sample block was removed using a solvent-rinsed rock hammer in the laboratory. The interior portion was then rinsed with dichloromethane (DCM) and allowed to dry. Samples were ground to a fine powder with solvent-rinsed mortar and pestle. Lipids were extracted from 40 to 200 g of powdered rock using a

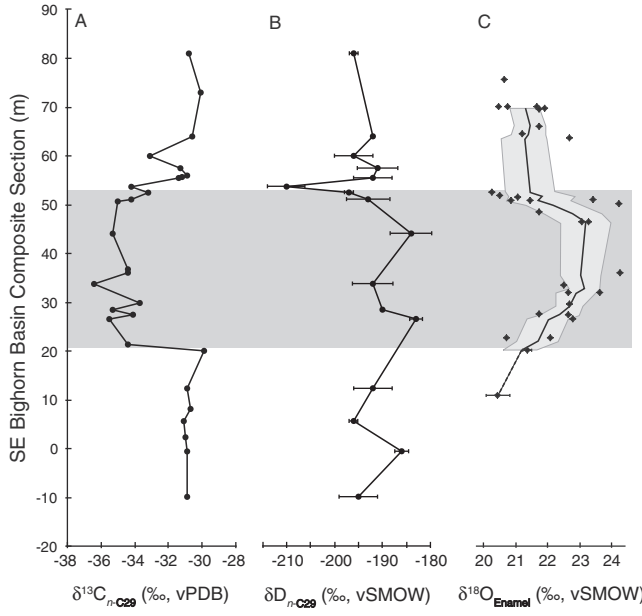

Fig. 2. Measured isotope ratios. (A) *n*-C_{29} $\delta^{13}C$ values (Baczynski et al., 2016), (B) *n*-C_{29} δD values (this study), error bars show standard error of the mean or standard deviation of replicate measurements (see Table 1), and (C) *Coryphodon* tooth enamel $\delta^{18}O$ values with a five-point moving average (black line) and shading indicating the 95% envelope of uncertainty (Secord et al., 2012).

Microwave Accelerated Reaction System (MARS Xpress, CEM Corporation) with 30 mL (9:1, v/v) DCM:methanol (MeOH) at 100 °C for 15 min. The total lipid extract (TLE) was filtered to remove sediment and concentrated under a stream of nitrogen gas using a TurboVap LV evaporator (Caliper Life Sciences). TLEs were separated into nonpolar and polar fractions by column chromatography using 1 g activated silica gel (70–230 mesh) in an ashed Pasteur pipet. The nonpolar constituent was eluted with 4 mL hexanes and the polar constituent with 4 mL (1:1, v/v) DCM:MeOH. Both fractions were concentrated under a stream of nitrogen using a nitrogen evaporator (N-Evap 112, Organomation Associates Inc.).

2.3. Lipid characterization

n-Alkanes were identified in the nonpolar fraction by gas chromatography–mass spectrometry (GC–MS) using a ThermoFisher Trace GC Ultra with a quadrapole mass spectrometer (ThermoFisher DSQII). A fused silica capillary column (Thermo Scientific TR5M5; 15 m long, 0.25 mm i.d., 0.25 μm film thickness) was used with helium as the carrier gas. The column flow rate was 1.5 mL/min. Samples were concurrently injected onto a second fused silica capillary column (Thermo Scientific TR5M5; 15 m long, 0.32 mm i.d., 0.25 μm film thickness) fitted to a flame ionization detector (FID) to determine relative abundance (column flow rate 3.0 mL/min). The GC oven temperature program began at 100 °C (held for 2 min) and then temperature was increased at a rate of 5 °C/min to a maximum temperature of 320 °C (held for 5 min). *n*-Alkanes were identified by confirming molecular ion mass and comparing *n*-alkane retention times with results from a standard mixture comprised of *n*-alkanes (*n*-C_{21} to *n*-C_{40}; Sigma Aldrich).

2.4. Compound-specific isotope analysis

Compound-specific stable hydrogen isotope ratios were measured at the University of Utah using a Thermo Trace 2000 GC coupled to a Finnigan Delta V isotope ratio mass spectrometer and high temperature pyrolysis furnace (1400 °C). The GC was fitted with a split/splitless injector operated in splitless mode with a fused silica column (Agilent J&W DB-5; 30 m, 0.25 mm, 0.25 μm). The column flow rate was 1.2 mL/min and the oven program began at a temperature of 102 °C (held for 4 min). Oven temperature then increased 6 °C/min to a maximum temperature of 350 °C with a final hold of 8 min. Isotopic abundances were determined relative to a reference gas calibrated with Mix A5 (*n*-C_{16} to *n*-C_{30}; Arndt Schimmelmann, Indiana University). Hydrogen isotope values of samples were normalized to the VSMOW scale using the Uncertainty Calculator (Polissar and D'Andrea, 2014) and are reported in standard delta notation. Standard errors of the mean for individual samples range from 3.9 to 4.8‰ (Table 1) (Uncertainty Calculator, Polissar and D'Andrea, 2014). The H_3^+ factor was measured daily (Sessions et al., 2001), and the average H_3^+ factor during the measurement period was 1.94 (SD = 0.03, n = 7).

2.5. Modeling annual precipitation isotope values

Precipitation isotope values are reconstructed using *Coryphodon* tooth enamel $\delta^{18}O$ values. The oxygen isotope composition of mammalian tooth enamel is controlled by the composition of an individual's diet and drinking water, and by its physiology (Bryant and Froelich, 1995; Kohn, 1996). Extant large-bodied, semi-aquatic, herbivorous mammals that are obligate drinkers dependably record local surface water $\delta^{18}O$ ratios and are insensitive to changes in relative humidity (Clementz et al., 2008; Levin et al., 2006). *Coryphodon*, an herbivorous mammal belonging to the extinct order Pantodonta, is the largest mammal in the Wyoming Paleogene fauna (340–700 kg; Uhen and Gingerich, 1995). Because *Coryphodon* is thought to have been a semi-aquatic hippopotamus ecomorph that was closely tied to water (Clementz et al., 2008; Secord et al., 2008; Simons, 1960), it should reliably track local surface water $\delta^{18}O$ values. *Coryphodon* teeth were collected from sixteen unique stratigraphic levels (4 pre-PETM, 6 PETM, 2 recovery, and 4 post-PETM) spanning roughly 100 m of section (Secord et al., 2012). *Coryphodon* stratigraphic levels were matched with *n*-alkane levels based on position within or between distinctive and laterally continuous marker beds that have been traced on foot across the field area. We caution that the magnitude of change between pre-PETM and PETM intervals reported here could be overestimated because of the small sample size, low sampling resolution, and the uncertainty introduced by comparing data from two proxy records sampled at different stratigraphic levels. To convert tooth enamel $\delta^{18}O$ values into precipitation $\delta^{18}O$ ratios, we use the empirical relationship between precipitation and tooth enamel phosphate from members of the sub-family Bovinae (Kohn and Dettman, 2007). Modifying for tooth enamel carbonate $\delta^{18}O$ values and solving for $\delta^{18}O_{precip}$ gives:

$$\delta^{18}O_{precip} = 1.08 * \delta^{18}O_{enamel(carbonate)}(\pm 0.03) - 35.27(\pm 0.3) \quad (1)$$

Precipitation δD values can then be estimated from $\delta^{18}O_{precip}$ values using an empirical relationship between $\delta^{18}O$ and δD values in modern precipitation, called the meteoric water line. The relationship observed at a global scale is termed the Global Meteoric Water Line (GMWL) (Craig, 1961):

$$\delta D_{precip} = 8 * \delta^{18}O_{precip} + 10 \quad (2)$$

However, the relationship between $\delta^{18}O$ and δD values in precipitation can deviate locally, generating a Local Meteoric Water Line (LMWL). LMWLs in particularly arid environments have slopes that are <8 (slope of GMWL) and y-intercepts that can vary significantly from that of the GMWL (Kendall and Coplen, 2001; Sharp, 2007). We model precipitation δD profiles two different ways to explore the potential effects of a change in meteoric water line. The first assumes a GMWL relationship (Eq. (1)) throughout the record. The second assumes the GMWL before and after the PETM, but uses a LMWL from an arid region

Table 1
n-Alkane sample name, local section meter level, interpolated composite curve meter level, δD values, uncertainty, and number of replicate measurements.

			$\delta D_{n\text{-alkane}}$								
			C_{27}			C_{29}			C_{31}		
Sample name	Local section meter level (m)	Interpolated composite curve meter level (m)	δD[b]	Uncertainty[c]	n	δD[b]	Uncertainty[c]	n	δD[b]	Uncertainty[c]	n
PP0904	HW 16/SCD; −9.8	−9.8				−195	4.0	3	−198	4.2	2
CAB3-04-06[a]	CAB 3; 18.5	−0.5				*−186*	*1.4*				
CAB3-04-07[a]	CAB 3; 24.7	5.7				*−196*	*0.9*				
FAS0803	HW 16; 12.4	12.4	−195	4.0	3	−192	4.0	3	−182	4.0	3
SW0801	HW 16; 12.4	12.4	−199	4.0	3	−197	4.0	3	−197	4.2	2
SW0803	HW 16; 12.4	12.4	−194	4.0	3	−192	4.0	3	−188	4.0	3
SW0904	HW 16; 12.4	12.4	−187	4.2	2	−186	4.2	2	−179	4.3	2
CAB7-04-02[a]	CAB 10; 20.7	26.6				*−183*	*1.3*				
CAB1-04-06[a]	CAB 10; 22.2	28.5				*−190*					
SW1003	CAB 10; 26.3	33.8	−190	4.2	2	−192	4.2	2	−189	4.2	2
SW1007	HW 16; 44.1	44.1	−185	4.8	1	−182	4.8	1	−184	4.8	1
SW0805	HW 16; 44.1	44.1	−177	4.3	2	−183	4.0	3	−183	4.0	3
SW0906	HW 16; 44.1	44.1	−187	4.2	2	−186	4.2	2	−189	4.2	2
SW0802	HW 16; 51.1	51.1	−190	4.2	2	−189	4.2	2	−183	4.2	2
SW1006	HW 16; 51.1	51.1	−198	4.8	1	−196	4.8	1	−190	4.8	1
CAB6-04-01[a]	CAB 10; 44.7	52.5				*−197*	*1.0*				
SW0813	HW 16; 53.7	53.7	−208	3.9	3	−210	3.9	3	−198	4.0	3
SW0907	BRS; 34	55.5	−194	4.0	3	−192	4.0	3	−187	4.0	3
SW1011	SCD; 45.5	57.5	−197	4.2	2	−191	4.2	2	−192	4.2	2
SW0817	HW 16; 60	60	−196	4.0	3	−196	4.0	3	−196	4.0	3
SW0306[1]	CAB 10; 54	64				*−192*	*0.3*				
CAB6-04-04[a]	CAB 10; 72.7	81.0				*−196*	*0.9*				

[a] Isotope data and uncertainty (reported as standard deviation) from Smith et al. (2007), m levels revised for interpolated composite curve.
[b] δD values on the VSMOW scale (‰), calculated using the Uncertainty Calculator spreadsheet (Polissar and D'Andrea, 2014), except for those in *italics* (see footnote a).
[c] Uncertainty of *n*-alkane δD values on the VSMOW scale (‰) reported as standard error of the mean, calculated using the Uncertainty Calculator spreadsheet (Polissar and D'Andrea, 2014), except for those in *italics* (see footnote a).

in the southwestern US (USGS drainage basin hydrologic unit code (HUC) 16, Kendall and Coplen, 2001) during the body of the PETM:

$$\delta D_{precip} = 4.9 * \delta^{18}O_{precip} - 42.2 \quad (3)$$

2.6. Modeling the influence of changes in apparent fractionation, ε_{app}

Plant taxonomic lineage can strongly influence apparent fractionation (ε_{app}) between source water and *n*-alkanes. We calculate ε_{app} using the *Coryphodon*-derived precipitation δD record and the C_{29} *n*-alkane δD record. Then, using an average apparent fractionation factor for modern monocots (−140‰) and dicots (−107‰) reported in the literature (Gao et al., 2014; Liu et al., 2016), we apply a binary mixing model to calculate the proportion of monocots required to produce the observed ε_{app} assuming that plant community change was the sole influence on apparent fractionation.

2.7. Modeling the influence of changes in season and amount of rainfall

Factors that influence the isotopic composition of precipitation include latitude, altitude, continentality, amount, and environmental parameters, such as temperature. Seasonal changes in temperature result in seasonal variation of isotopic composition of precipitation, except at low latitudes where there is little change in temperature throughout the year (Dansgaard, 1964). Temperature influences both the amount of water that air can hold and the fractionation between water vapor and condensate. This manifests in higher precipitation isotope values during the summer and lower precipitation isotope values during the winter. Taking the isotopic composition of *Coryphodon* tooth enamel as a record of the amount-weighted isotopic composition of mean annual precipitation, we use a mass balance calculation to determine the possible range of seasonal precipitation isotope values for two end-member scenarios: one in which all precipitation falls during the cool season and the other in which all precipitation falls during the warm season. We use variability in *Coryphodon* and *Ectoganus* intra-tooth $\delta^{18}O$ ratios (R. Secord, unpublished data; Fricke et al., 1998) to constrain pre-PETM seasonal δD variability to 24‰ and PETM seasonal variability to 12‰ (see Supplement for details). Mean annual precipitation (MAP) was approximated using estimates from the CALMAG soil weathering index (a method of quantitatively assessing rainfall amount in vertisols (Kraus et al., 2013; Nordt and Driese, 2010)) and leaf area analysis of paleofloras in the southeastern Bighorn Basin (Kraus et al., 2013; Peppe et al., 2011; Wing et al., 2005). We use 1400 mm and 800 mm annual rainfall for pre-PETM and PETM conditions, respectively.

Evidence from modern plants indicates that leaf wax *n*-alkane production is seasonally biased, occurring only during a short portion of the year, rather than year-round (Kahmen et al., 2011; Sachse et al., 2010; Sachse et al., 2009; Tipple et al., 2013). The modeled seasonal variation in precipitation δD values is used to determine how changes in the season of leaf-wax production during the PETM could generate the observed leaf wax δD record.

3. Results

3.1. n-Alkane δD ratios

Twenty-two of the 36 samples contained leaf wax *n*-alkanes abundant enough for hydrogen isotope analysis (Table 1). Hydrogen isotope values range between −177 and −210‰. δD values of the *n*-C_{27}, *n*-C_{29} and *n*-C_{31} chain lengths within a single sample vary up to 12‰ (Table 1). We restrict further data analysis to the *n*-C_{29} chain length, which has the highest resolution δD record. These new and published hydrogen isotope values (Smith et al., 2007) (Table 1) from plant localities in the southeastern Bighorn Basin, Wyoming (Fig. 1) have been projected onto a single, interpolated composite curve (Fig. 2B; see also Baczynski et al., 2013).

3.2. Precipitation isotope values

Coryphodon tooth enamel $\delta^{18}O$ values range between 21.5 and 25.2‰ (Fig. 2C; Table 2). Precipitation $\delta^{18}O$ values, calculated from *Coryphodon* $\delta^{18}O$ values (Fig. 3A) using Eq. (1), fall between −12.1

Table 2
Isotope ratios, apparent fractionation ($\varepsilon_{wax\text{-}precip}$), and proportion monocot. *n*-Alkane δD values are matched with *Coryphodon* tooth enamel $\delta^{18}O$ values from equivalent stratigraphic levels. $\delta^{18}O_{precip}$ is calculated using an empirical relationship between tooth enamel and precipitation values using equation 1. δD_{precip} (GMWL) uses the GMWL relationship (Eq. (2)) for the entire record. δD_{precip} (LMWL) is calculated using the GMWL relationship before and after the PETM, and a LMWL (Eq. (3)) during the PETM. The fractionation factor between leaf wax and precipitation ($\varepsilon_{wax\text{-}precip}$) is calculated using *n*-alkane δD and *Coryphodon*-derived δD_{precip}. The proportion of monocot required to generate $\varepsilon_{wax\text{-}precip}$ is calculated assuming an average monocot (−140‰) and dicot (−107‰) $\varepsilon_{wax\text{-}precip}$ value.

PETM phase	Plant quarry ID	Meter level (m)	*n*-Alkane $\delta D_{n\text{-}C29}$ (‰)	*Coryphodon* $\delta^{18}O_{enamel}$ (‰)	$\delta^{18}O_{precip\ (‰)}$	δD_{precip} (GMWL) (‰)	δD_{precip} (LMWL) (‰)	$\varepsilon_{wax\text{-}precip}$	Proportion monocot
Post	CAB6-04-04	81.0	−196	22.4	−11.2	−79.2	−79.2	−127	0.6
Post	SW0306	64.0	−192	22.4	−11.2	−79.2	−79.2	−123	0.5
Post	SW0817	60.0	−196	22.4	−11.2	−79.2	−79.2	−127	0.6
Post	SW1011	57.5	−191	22.4	−11.2	−79.2	−79.2	−121	0.4
Recovery	SW 0907	55.5	−192	21.6	−12.0	−86.1	−86.1	−116	0.3
Recovery	SW0813	53.7	−210	21.6	−12.0	−86.1	−86.1	−136	0.9
PETM	CAB6-04-01	52.5	−197	23.5	−10.0	−69.7	−91.0	−137	0.9
PETM	SW0802/1006	51.1	−192	23.5	−10.0	−69.7	−91.0	−131	0.7
PETM	SW0805/0906/1007	44.1	−184	25.2	−8.1	−55.0	−82.0	−136	0.9
PETM	SW1003	33.8	−192	23.9	−9.5	−66.2	−88.9	−135	0.8
PETM	CAB1-04-06	28.5	−190	23.3	−10.2	−71.4	−92.1	−128	0.6
PETM	CAB7-04-02	26.6	−183	23.3	−10.2	−71.4	−92.1	−120	0.4
Pre	SW0801/0803/0904	12.4	−192	21.5	−12.1	−86.9	−86.9	−115	0.2
Pre	CAB3-04-07	5.7	−196	21.5	−12.1	−86.9	−86.9	−119	0.4
Pre	CAB3-04-06	−0.5	−186	21.5	−12.1	−86.9	−86.9	−109	0.0
Pre	PP0904	−9.8	−195	21.5	−12.1	−86.9	−86.9	−118	0.3

and −8.1, revealing a positive ~4‰ shift during the PETM (Fig. 3B). When the GMWL (Eq. (2)) is used to estimate precipitation δD ratios, values range from −87‰ to −55‰ (Table 2, Fig. 3C). When we apply the arid-land LMWL (Eq. (3)) during the PETM body and the GMWL pre- and post-PETM, the resulting precipitation δD record shows little change across the PETM, with δD values varying between −92‰ and −79‰ (Table 2, Fig. 3D).

3.3. Apparent fractionation between precipitation and leaf wax lipids

Apparent fractionation between the hydrogen isotope ratios of annual precipitation and C_{29} *n*-alkane ranges between −109‰ and −137‰ (Table 2, Fig. 4C). The average pre-PETM apparent fractionation is −115‰, and the average PETM ε_{app} is −132‰. Using an average monocot ε_{app} of −140‰ and average dicot ε_{app} of −107‰, we calculate that monocots would have to comprise 30% of the pre-PETM floral assemblage and 80–90% of the PETM flora to produce the observed PETM ε_{app} values (Fig. 4D).

3.4. Season of rainfall and production of n-alkanes

The modeled range of seasonal precipitation isotope values that conforms to the constraints imposed by *Coryphodon* tooth enamel oxygen isotopes and estimates of MAP in the Bighorn Basin is shown in Fig. 5. The hashed region marks the range of precipitation δD overlap between pre-PETM (blue) and PETM (red) scenarios (−79‰ to −63‰). Thus, even though the hydrogen isotopic composition of mean annual precipitation changed significantly during the PETM (dashed blue and red lines Fig. 5), pre-PETM and PETM precipitation is isotopically identical under certain conditions. If *n*-alkanes record precipitation isotope ratios

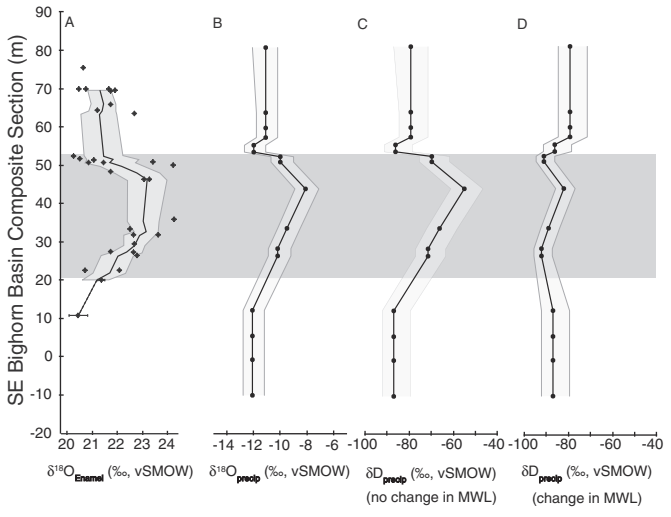

Fig. 3. Measured and calculated isotope ratios. (A) Measured *Coryphodon* tooth enamel $\delta^{18}O$ values (Secord et al., 2012), same as Fig. 2C, (B) precipitation $\delta^{18}O$ values, calculated by applying an empirical relationship between tooth enamel and precipitation $\delta^{18}O$ values from members of the modern sub-family Bovinae (Kohn and Dettman, 2007), (C) precipitation δD values calculated from B using the GMWL relationship, and (D) precipitation δD values calculated from B using GMWL pre- and post-PETM and an arid-land LMWL relationship during the PETM. Gray envelopes for B–D represent the range of possible values accounting for the uncertainty associated with Equation 1.

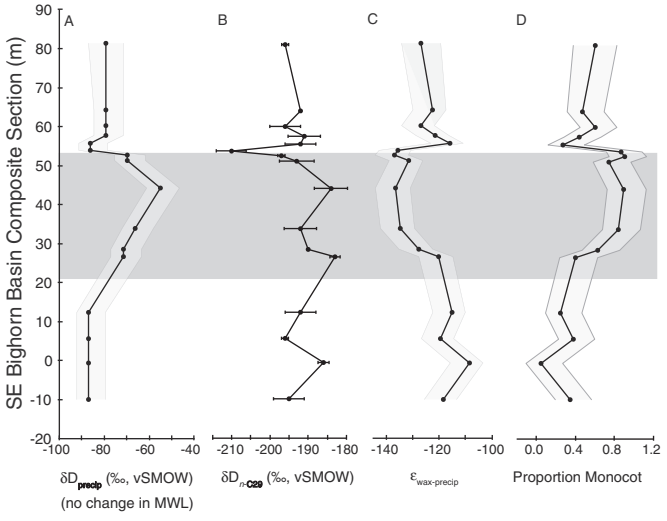

Fig. 4. Isotope ratios, apparent fractionation ($\varepsilon_{wax\text{-}precip}$), and proportion monocots. (A) Precipitation δD values calculated using the GMWL relationship, same as Fig. 3C, (B) measured *n*-alkane δD values, same as Fig. 2A, error bars show standard error of the mean or standard deviation of replicate measurements (see Table 1), (C) apparent fractionation ($\varepsilon_{wax\text{-}precip}$) factor calculated using A and B, and (D) the proportion monocot required to generate C, using an average monocot (−140‰) and average dicot (−107‰) $\varepsilon_{wax\text{-}precip}$ value from the literature (Liu et al., 2016). Gray envelopes for A, C, and D represent the range of possible values accounting for the uncertainty associated with Equation 1.

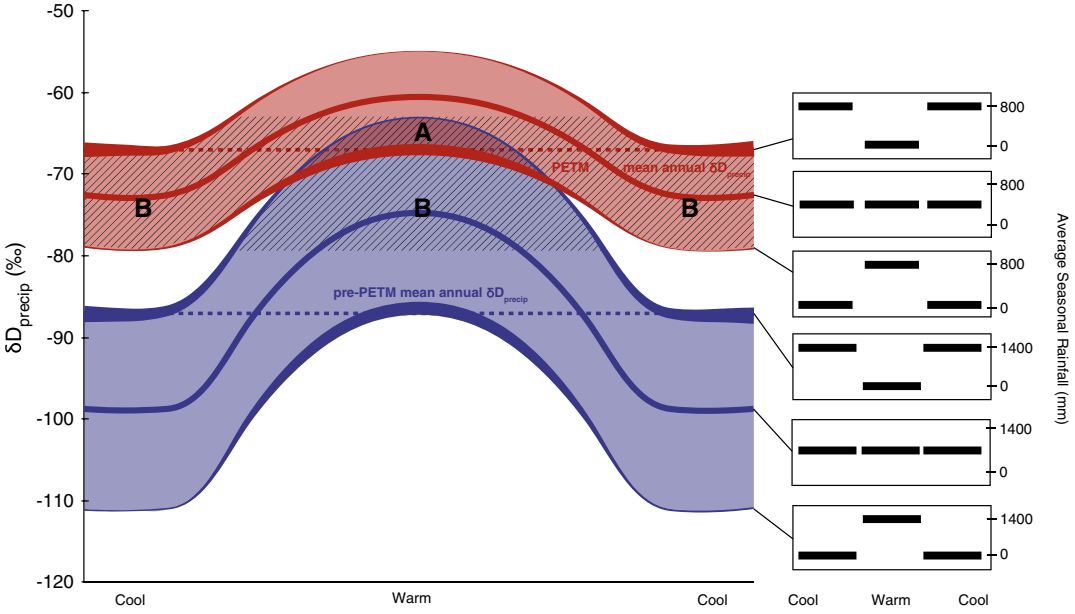

Fig. 5. Seasonal (cool vs. warm) variation in precipitation amount and isotopic values for pre-PETM (blue) and PETM (red) with reduced seasonal isotope range during the PETM. Line thickness represents relative precipitation amount with seasonal average rainfall amounts indicated with panels at right. Upper and lower lines of seasonal rainfall isotope ratios depict end-member scenarios: upper red and blue lines, all precipitation falls during the cool season and lower red and blue lines, all precipitation falls during the warm season. The middle red and blue lines show precipitation evenly distributed between warm and cool season. The dashed lines represent the amount-weighted mean annual precipitation isotope values calculated using *Coryphodon* tooth enamel. The hashed region shows the area of pre-PETM and PETM isotope overlap. The tooth enamel and *n*-alkane isotope records can be reconciled if (A) there was a change in the season of rainfall from the cool season pre-PETM to the warm season in the PETM but no change in the season of lipid production or (B) if there was a shift in the season of lipid production (warm pre-PETM to cool PETM).

from just a portion of the year, specifically during the part of the year in which pre-PETM and PETM precipitation isotope ratios were indistinguishable (hashed region Fig. 5), then *Coryphodon* and *n*-alkane isotope records can be reconciled. For pre-PETM and PETM precipitation δD ratios to be similar, there had to have been either a change in the season of rainfall (Scenario A, Fig. 5) or a shift in the season of lipid production (Scenario B, Fig. 5). For example, if pre-PETM *n*-alkanes recorded precipitation during a warm dry season, and PETM *n*-alkanes recorded precipitation during a warm wet season, there would be no change in *n*-alkane δD ratios across the PETM (Scenario A, Fig. 5). These conditions would be met if the season of rainfall shifted from the cool season pre-PETM to the warm season during the PETM. Alternatively, a shift in the season of lipid production could also result in negligible change in *n*-alkane δD values during the PETM, if pre-PETM *n*-alkanes were synthesized during the warmer season and PETM *n*-alkanes were produced during the cooler season (Scenario B, Fig. 5).

4. Discussion

The *Coryphodon*-derived precipitation $\delta^{18}O$ and *n*-alkane δD profiles show two different patterns. The precipitation $\delta^{18}O$ record (Fig. 2C) displays a relatively simple increase to an alternate semi-stable state during the PETM whereas *n*-alkane hydrogen isotope ratios show no clear shift during the PETM (Fig. 2B). Source water, plant physiology, and relative humidity are all factors known to influence the hydrogen isotope ratios of *n*-alkanes. While it is possible that an increase in relative humidity of 20–30% could compensate for an increase in precipitation δD values (Craig-Gordon calculation, see Supplement for details), we do not consider this hypothesis further because the direction of change is opposite of what we expect based on all other proxy data from the Bighorn Basin (Kraus et al., 2013; Secord et al., 2012; Smith et al., 2007; Wing et al., 2005). We instead consider the more likely scenarios that floral turnover effected a shift in the apparent fractionation between leaf wax and precipitation, or that source water hydrogen isotope ratios changed, either due to a change in the local meteoric water line or because of a change in the season of rainfall or season of lipid production.

Leaf fossils from the Bighorn Basin indicate that the plant community shifted from a mixed angiosperm/conifer flora to predominantly angiosperms during the PETM (Smith et al., 2007; Wing et al., 2005). The local extirpation of conifers should not have affected ε_{app} because modern conifers and angiosperm dicots show similar apparent fractionation factors (Bi et al., 2005; Chikaraishi and Naraoka, 2003; Sachse et al., 2006). However, there is a notable difference in apparent fractionation within angiosperms between monocots and dicots, and fossil evidence suggests that there was an increase in the number of monocots during the early part of the CIE. We calculate that monocots would have to comprise 30% of the flora before the PETM and 80–90% during PETM to produce the observed PETM ε_{app} values (Fig. 4D). Monocots were largely absent prior to the PETM and were not more abundant than dicots during the PETM (Wing and Currano, 2013). Palms are also concentrated in the lower part of the CIE and do not support a step-wise increase in monocots for the duration of the PETM. Moreover, limited data from five modern palm species closely-related to those present during the PETM show a wide range of biosynthetic fractionation factors, some of which are similar to the average monocot value and some of which are similar to the dicot average (Gao et al., 2014). While floral change and its effect on fractionation might have played a minor role, available evidence suggests that this alone could not compensate for a shift in precipitation δD values.

Alternatively, a change in source water hydrogen isotope ratios could reconcile the *Coryphodon* and *n*-alkane isotope records. If the slope of the LMWL decreased during the PETM, it is possible to produce a precipitation record with negligible change in δD across the PETM (Fig. 3D). If pre-PETM and PETM plants expressed similar apparent fractionation, the resulting *n*-alkane record would also show little change across the PETM, much like the measured *n*-alkane δD record. The model that generated a δD profile closest to the observed data used the GMWL pre- and post-PETM but during the PETM, applied the LMWL relationship for USGS drainage basin HUC 16, which encompasses much of Utah and

Nevada (Kendall and Coplen, 2001). HUC 16 has a slope of 4.9, considerably lower than that of the GMWL and the smallest slope of all 21 HUCs. Such an extreme LMWL exists only in the most arid environments, which is inconsistent with proxy data for the PETM in the Bighorn Basin. Floral, faunal, sedimentological, and geochemical data suggest that the PETM was drier or more seasonally arid than the late Paleocene, but that PETM MAP was at least 800 mm, less arid than the LMWL from the southwest US would imply. Therefore, a change in LMWL is unlikely to fully resolve the differences between the *n*-alkane and *Coryphodon* isotope records.

The previous two hypotheses assume that plants derived water from the same annually averaged precipitation recorded in the *Coryphodon* tooth enamel. However, leaf wax *n*-alkanes may record a seasonally biased rather than year-round signal. Some studies suggest that leaf wax *n*-alkanes record the plant-water environment at the time of leaf flush or early in the growing season (Kahmen et al., 2011; Sachse et al., 2010; Tipple et al., 2013) while others suggest a bias towards the end of the growing season (Gao et al., 2012; Sachse et al., 2009). Although the season itself remains under debate, there is a growing consensus that *n*-alkanes record only a small fraction of the annual climate signal. If we interpret the *n*-alkanes as a record of seasonal precipitation rather than average annual precipitation, the dissimilarity between the *n*-alkane and *Coryphodon* isotope records can be explained by a change in either the season of rainfall or the season of lipid production.

Located at a paleolatitude of ~49°N, annual changes in insolation would have caused precipitation in the Bighorn Basin during the Paleogene to exhibit seasonal variation in isotopic values, in spite of overall warmer temperatures. Nonetheless, the range of seasonal extremes in isotopic composition of precipitation could have been reduced due to the warming of the PETM. In fact, preliminary oxygen isotope data from serial sampling of mammalian tooth enamel suggest a decrease in seasonality of precipitation $\delta^{18}O$ values during the PETM, although sample size is too small to test for significance. Variability in mammalian tooth enamel $\delta^{18}O$ values tends to underestimate the isotopic variability of precipitation, representing a minimum range of precipitation isotopic values. Nevertheless, we use these constraints as a starting point to explore how changes in seasonality could influence *Coryphodon* and *n*-alkane isotope ratios. By varying the seasonal distribution of precipitation, we find that pre-PETM and PETM precipitation δD values could have been similar during particular times of the year despite having different annual averages (Fig. 5).

The pre-PETM and PETM isotopic ranges have a small area of direct overlap during the warm season (Scenario A, Fig. 5). In addition to *n*-alkanes recording warm season precipitation, option A also requires that the season of rainfall change from the cool season before the PETM to the warm season during the PETM. Alternatively, a shift in the season of lipid production, from warm season pre-PETM to cool season during the PETM (Scenario B, Fig. 5), could also produce *n*-alkanes with identical δD ratios, because precipitation δD ratios would be the same during lipid formation despite a shift in mean annual precipitation amount and isotopic composition. This result is insensitive to whether a shift in the seasonal range of precipitation isotope ratios is assumed to decrease during the PETM (Fig. 5) or stay the same (Fig. S3).

Because of the probable seasonal bias of *n*-alkanes, we posit that the most likely explanation for the decoupling of the *Coryphodon* and *n*-alkane isotope records is that the season of rainfall or lipid production changed during the PETM. Either of these changes seem equally plausible. Although global circulation model results can differ immensely, some have predicted a monsoon-like PETM climate, with greater rainfall delivery to the western interior of North America from the Mississippi Embayment during the summer months (Winguth et al., 2010). Alternatively, extreme summer heat and soil dryness could have inhibited plant growth. Warmer "cool season" temperatures, however, could have expanded the duration of the growing season during the PETM, opening up possibilities for plants to flush during the cooler season or whenever precipitation was sufficient to promote growth.

5. Conclusions

Using both leaf-wax *n*-alkane hydrogen and mammalian tooth enamel oxygen isotope data from the same field area, this study is unique in its ability to interpret the leaf wax δD record with an independent constraint on precipitation isotope ratios. We considered several possible hypotheses, modeled the changes that would have been necessary to produce the observed isotopic records, and evaluated the likelihood of each. We conclude that the extreme changes in the LMWL or apparent fractionation required to reconcile the tooth enamel and lipid isotope records renders these scenarios untenable. It is more likely that the difference between the *n*-alkane δD record and *Coryphodon* $\delta^{18}O$ record is due to a shift in either the season of rainfall or season of lipid production. Such a change is consistent with the growing body of evidence that suggests precipitation became more seasonal or episodic in response to the PETM temperature increase. Our results, at the very least, underscore the problems associated with interpreting lipid δD records without knowledge of precipitation isotope values, and may imply that plants adapted to the PETM temperature increase by shifting their season of leaf flush to the cooler part of the year.

Supplementary data to this article can be found online at http://dx.doi.org/10.1016/j.palaeo.2016.10.030.

Acknowledgements

We are grateful to Jim Ehleringer, Brett Tipple, Melissa Berke, and Bastian Hambach for their generosity and assistance in the SIRFER laboratory, Paul Morse for assistance with Fig. 1, and Rosemary Bush for helpful scientific discussions. We thank Doug Boyer for his tremendous effort tracing beds and compiling GIS data throughout the field area over the past decade that has contributed to the stratigraphy that ties this data together. The manuscript benefitted greatly from the thoughtful comments from two anonymous reviewers and the editor Isabel Montañez. Funding was provided by NSF awards EAR-0720268 (FAM), EAR-0717892 (SLW), EAR-0718740 (MJK), EAR-0640076 (JIB, J. Krigbaum, R. Secord), EAR-0719941 (JIB), Initiative for Sustainability and Energy at Northwestern, and Australian Research Council FT110100100791, DP130104314 (FAM). Vertebrate fossils were collected under the Bureau of Land Management permits to JIB (PA04-WY-113, PA10-WY-185).

References

Baczynski, A.A., McInerney, F.A., Wing, S.L., Kraus, M.J., Bloch, J.I., Boyer, D.M., Secord, R., Morse, P.E., Fricke, H.C., 2013. Chemostratigraphic implications of spatial variation in the Paleocene-Eocene thermal maximum carbon isotope excursion, SE Bighorn Basin, Wyoming. Geochem. Geophys. Geosyst. 14, 4133–4152.

Baczynski, A.A., McInerney, F.A., Wing, S.L., Kraus, M.J., Morse, P.E., Bloch, J.I., Chung, A.H., Freeman, K.H., 2016. Distortion of carbon isotope excursion in bulk soil organic matter during the Paleocene-Eocene thermal maximum. Geol. Soc. Am. Bull.

Betts, R.A., Boucher, O., Collins, M., Cox, P.M., Falloon, P.D., Gedney, N., Hemming, D.L., Huntingford, C., Jones, C.D., Sexton, D.M.H., Webb, M.J., 2007. Projected increase in continental runoff due to plant responses to increasing carbon dioxide. Nature 448, 1037–1041.

Bi, X.H., Sheng, G.Y., Liu, X.H., Li, C., Fu, J.M., 2005. Molecular and carbon and hydrogen isotopic composition of *n*-alkanes in plant leaf waxes. Org. Geochem. 36, 1405–1417.

Bowen, G.J., Beerling, D.J., Koch, P.L., Zachos, J.C., Quattlebaum, T., 2004. A humid climate state during the Palaeocene/Eocene thermal maximum. Nature 432, 495–499.

Bowen, G.J., Bowen, B.B., 2008. Mechanisms of PETM global change constrained by a new record from central Utah. Geology 36, 379–382.

Bown, T.M., 1980. Summary of latest Cretaceous and Cenozoic sedimentary, tectonic, and erosional events, Bighorn Basin, Wyoming. In: Gingerich, P.D. (Ed.), Early Cenozoic Paleontology and Stratigraphy of the Bighorn Basin. University of Michigan Ann Arbor, Wyoming, pp. 25–32.

Bryant, D.J., Froelich, P.N., 1995. A model of oxygen isotope fractionation in body water of large mammals. Geochim. Cosmochim. Acta 59, 4523–4537.

Cao, L., Bala, G., Caldeira, K., Nemani, R., Ban-Weiss, G., 2010. Importance of carbon dioxide physiological forcing to future climate change. Proc. Natl. Acad. Sci. 107, 9513–9518.

Chikaraishi, Y., Naraoka, H., 2003. Compound-specific dD-d13C analyses of *n*-alkanes extracted from terrestrial and aquatic plants. Phytochemistry 63, 361–371.

Ciais, P., Sabine, C., Bala, G., Bopp, L., Brovkin, V., Canadell, J., Chhabra, A., DeFries, R., Galloway, J., Heimann, M., Jones, C., Le Quéré, C., Myneni, R.B., Piao, S., Thornton, P., 2013. Carbon and other biogeochemical cycles. In: Stocker, T.F., Qin, D., Plattner, G.-

K., Tignor, M., Allen, S.K., Boschung, J., Nauels, A., Xia, Y., Bex, V., Midgley, P.M. (Eds.), Climate Change 2013: The Physical Science Basis. Contribution of Working Group I to the Fifth Assessment Report of the Intergovernmental Panel on Climate Change. Cambridge University Press, Cambridge, United Kingdom and New York, NY, USA .

Clementz, M.T., Holroyd, P.A., Koch, P.L., 2008. Identifying aquatic habits of herbivorous mammals through stable isotope analysis. PALAIOS 23, 574–585.

Collins, M., Knutti, R., Arblaster, J., Dufresne, J.-L., Fichefet, T., Friedlingstein, P., Gao, X., Gutowski, W.J., Johns, T., Krinner, G., Shongwe, M., Tebaldi, C., Weaver, A.J., Wehner, M., 2013. Long-term climate change: projections, commitments and irreversibility. In: Stocker, T.F., Qin, D., Plattner, G.K., Tignor, M., Allen, S.K., Boschung, J., Nauels, A., XIa, Y., Bex, V., Midgley, P.M. (Eds.), Climate Change 2013: The Physcial Science Basis. Contribution of Working Group I to the Fifth Assessment Report of the Intergovernmental Panel on Climate Change. Cambridge University Press, Cambridge, United Kingdom and New York, NY, USA .

Craig, H., 1961. Isotopic variations in meteoric waters. Science 133, 1702–1703.

Craig, H., Gordon, L.I., 1965. Deuterium and oxygen-18 variations in the ocean and the marine atmosphere. In: Tongiorgi, E. (Ed.), Proceedings of the Third Spoletto Conference on Stable Isotopes in Oceanographic Studies and Paleotemperatures. CNR-Laboratorio di Geologia Nucleare, pp. 9–130.

Cramer, B.S., Aubry, M.P., Miller, K.G., Olsson, R.K., Wright, J.D., Kent, D.V., 1999. An exceptional chronologic, isotopic, and clay mineralogic record of the latest Paleocene thermal maximum, Bass River, NJ, ODP 174AX. Bull. Soc. Geol. Fr. 170, 883–897.

Crouch, E.M., Dickens, G.R., Brinkhuis, H., Aubry, M.P., Hollis, C.J., Rogers, K.M., Visscher, H., 2003. The Apectodinium acme and terrestrial discharge during the Paleocene-Eocene Thermal Maximum: new palynological, geochemical and calcareous nannoplankton observations at Tawanui, New Zealand. Palaeogeogr. Palaeoclimatol. Palaeoecol. 194, 387–403.

Dansgaard, W., 1964. Stable isotopes in precipitation. Tellus 16, 436–468.

Eglinton, G., Hamilton, R.J., 1967. Leaf Epicuticular Waxes. Science 156, 1322–1335.

Foreman, B.Z., Heller, P.L., Clementz, M.T., 2012. Fluvial response to abrupt global warming at the Palaeocene/Eocene boundary. Nature 491, 92–95.

Fricke, H.C., Clyde, W.C., O'Neil, J.R., 1998. Intra-tooth variations in delta O-18 (PO4) of mammalian tooth enamel as a record of seasonal variations in continental climate variables. Geochim. Cosmochim. Acta 62, 1839–1850.

Gao, L., Edwards, E.J., Zeng, Y., Huang, Y., 2014. Major evolutionary trends in hydrogen isotope fractionation of vascular plant leaf waxes. PLoS One 9, e112610.

Gao, L., Tsai, Y.-J., Huang, Y., 2012. Assessing the rate and timing of leaf wax regeneration in *Fraxinus americana* using stable hydrogen isotope labeling. Rapid Commun. Mass Spectrom. 26, 2241–2250.

Garel, S., Schnyder, J., Jacob, J., Dupuis, C., Boussafir, M., Le Milbeau, C., Storme, J.Y., Iakovleva, A.I., Yans, J., Baudin, F., Flehoc, C., Quesnel, F., 2013. Paleohydrological and paleoenvironmental changes recorded in terrestrial sediments of the Paleocene-Eocene boundary (Normandy, France). Palaeogeogr. Palaeoclimatol. Palaeoecol. 376, 184–199.

Gat, J.R., 1996. Oxygen and hydrogen isotopes in the hydrologic cycle. Annu. Rev. Earth Planet. Sci. 24, 225–262.

Gibson, T.G., Bybell, L.M., Mason, D.B., 2000. Stratigraphic and climatic implications of clay mineral changes around the Paleocene/Eocene boundary of the northeastern US margin. Sediment. Geol. 134, 65–92.

Handley, L., Crouch, E.M., Pancost, R.D., 2011. A New Zealand record of sea level rise and environmental change during the Paleocene-Eocene Thermal Maximum. Palaeogeogr. Palaeoclimatol. Palaeoecol. 305, 185–200.

Handley, L., Pearson, P.N., McMillan, I.K., Pancost, R.D., 2008. Large terrestrial and marine carbon and hydrogen isotope excursions in a new Paleocene/Eocene boundary section from Tanzania. Earth Planet. Sci. Lett. 275, 17–25.

Huber, M., Sloan, L.C., 1999. Warm climate transitions: a general circulation modeling study of the Late Paleocene thermal maximum (about 56 Ma). J. Geophys. Res.-Atmos. 104, 16633–16655.

Jaramillo, C., Ochoa, D., Contreras, L., Pagani, M., Carvajal-Ortiz, H., Pratt, L.M., Krishnan, S., Cardona, A., Romero, M., Quiroz, L., Rodriguez, G., Rueda, M.J., de la Parra, F., Moron, S., Green, W., Bayona, G., Montes, C., Quintero, O., Ramirez, R., Mora, G., Schouten, S., Bermudez, H., Navarrete, R., Parra, F., Alvaran, M., Osorno, J., Crowley, J.L., Valencia, V., Vervoort, J., 2010. Effects of rapid global warming at the Paleocene-Eocene boundary on neotropical vegetation. Science 330, 957–961.

Kahmen, A., Dawson, T.E., Vieth, A., Sachse, D., 2011. Leaf wax *n*-alkane delta D values are determined early in the ontogeny of *Populus trichocarpa* leaves when grown under controlled environmental conditions. Plant Cell Environ. 34, 1639–1651.

Kahmen, A., Hoffmann, B., Schefuss, E., Arndt, S.K., Cernusak, L.A., West, J.B., Sachse, D., 2013a. Leaf water deuterium enrichment shapes leaf wax *n*-alkane delta D values of angiosperm plants II: observational evidence and global implications. Geochim. Cosmochim. Acta 111, 50–63.

Kahmen, A., Schefuss, E., Sachse, D., 2013b. Leaf water deuterium enrichment shapes leaf wax *n*-alkane delta D values of angiosperm plants I: experimental evidence and mechanistic insights. Geochim. Cosmochim. Acta 111, 39–49.

Kaiho, K., Arinobu, T., Ishiwatari, R., Morgans, H.E.G., Okada, H., Takeda, N., Tazaki, K., Zhou, G.P., Kajiwara, Y., Matsumoto, R., Hirai, A., Niitsuma, N., Wada, H., 1996. Latest paleocene benthic foraminiferal extinction and environmental changes at Tawanui, New Zealand. Paleoceanography 11, 447–465.

Kendall, C., Coplen, T.B., 2001. Distribution of oxygen-18 and deuterium in river waters across the United States. Hydrol. Process. 15, 1363–1393.

Kennett, J.P., Stott, L.D., 1991. Abrupt deep-sea warming, palaeoceanographic changes and benthic extinctions at the end of the Palaeocene. Nature 353, 225–229.

Kohn, M.J., 1996. Predicting animal δ18O: accounting for diet and physiological adaptation. Geochim. Cosmochim. Acta 60, 4811–4829.

Kohn, M.J., Dettman, D.L., 2007. Paleoaltimetry from stable isotope compositions of fossils. Rev. Mineral. Geochem. 66, 119–154.

Kraus, M.J., McInerney, F.A., Wing, S.L., Secord, R., Baczynski, A.A., Bloch, J.I., 2013. Paleohydrologic response to continental warming during the Paleocene-Eocene thermal maximum, Bighorn Basin, Wyoming. Palaeogeogr. Palaeoclimatol. Palaeoecol. 370, 196–208.

Kraus, M.J., Riggins, S., 2007. Transient drying during the Paleocene-Eocene Thermal Maximum (PETM): analysis of paleosols in the Bighorn Basin, Wyoming. Palaeogeogr. Palaeoclimatol. Palaeoecol. 245, 444–461.

Krishnan, S., Pagani, M., Agnini, C., 2015. Leaf waxes as recorders of paleoclimatic changes during the Paleocene–Eocene Thermal Maximum: regional expressions from the Belluno Basin. Org. Geochem. 80, 8–17.

Levin, N.E., Cerling, T.E., Passey, B.H., Harris, J.M., Ehleringer, J.R., 2006. A stable isotope aridity index for terrestrial environments. Proc. Natl. Acad. Sci. U. S. A. 103, 11201–11205.

Liu, J., Liu, W., An, Z., Yang, H., 2016. Different hydrogen isotope fractionations during lipid formation in higher plants: implications for paleohydrology reconstruction at a global scale. Sci. Rep. 6, 19711.

McInerney, F.A., Wing, S.L., 2011. The Paleocene-Eocene Thermal Maximum: a perturbation of carbon cycle, climate, and biosphere with implications for the future. Annu. Rev. Earth Planet. Sci. 39, 489–516.

Nordt, L.C., Driese, S.D., 2010. New weathering index improves paleorainfall estimates from vertisols. Geology 38, 407–410.

Pagani, M., Pedentchouk, N., Huber, M., Sluijs, A., Schouten, S., Brinkhuis, H., Damste, J.S.S., Dickens, G.R., Scientists, E., 2006. Arctic hydrology during global warming at the Palaeocene/Eocene Thermal Maximum. Nature 442, 671–675.

Pedentchouk, N., Freeman, K.H., Harris, N.B., 2006. Different response of delta D values of *n*-alkanes, isoprenoids, and kerogen during thermal maturation. Geochim. Cosmochim. Acta 70, 2063–2072.

Peppe, D.J., Royer, D.L., Cariglino, B., Oliver, S.Y., Newman, S., Leight, E., Enikolopov, G., Fernandez-Burgos, M., Herrera, F., Adams, J.M., Correa, E., Currano, E.D., Erickson, J.M., Hinojosa, L.F., Hoganson, J.W., Iglesias, A., Jaramillo, C.A., Johnson, K.R., Jordan, G.J., Kraft, N.J.B., Lovelock, E.C., Lusk, C.H., Niinemets, U., Penuelas, J., Rapson, G., Wing, S.L., Wright, I.J., 2011. Sensitivity of leaf size and shape to climate: global patterns and paleoclimatic applications. New Phytol. 190, 724–739.

Polissar, P.J., D'Andrea, W.J., 2014. Uncertainty in paleohydrologic reconstructions from molecular δD values. Geochim. Cosmochim. Acta 129, 146–156.

Robert, C., Kennett, J.P., 1994. Antarctic subtropical humid episode at the Paleocene-Eocene boundary — clay-mineral evidence. Geology 22, 211–214.

Rose, K.D., Chew, A.E., Dunn, R.H., Kraus, M.J., Fricke, H.C., Zack, S.P., 2012. Earliest Eocene mammalian fauna from the Paleocene-Eocene Thermal Maximum at Sand Creek Divide, Southern Bighorn Basin, Wyoming. Univ. Michigan Pap. Paleontol. 36, 1–122.

Rozanski, K., Araguas-Araguas, L., Gonfiantini, R., 1993. Isotopic patterns in modern global precipitation. In: Swart, P.K., Lohmann, K.C., McKenzie, J., Savin, S. (Eds.), Climate Change in Continental Isotopic Records. American Geophysical Union, pp. 1–36.

Sachse, D., Billault, I., Bowen, G.J., Chikaraishi, Y., Dawson, T.E., Feakins, S.J., Freeman, K.H., Magill, C.R., McInerney, F.A., van der Meer, M.T.J., Polissar, P., Robins, R.J., Sachs, J.P., Schmidt, H.L., Sessions, A.L., White, J.W.C., West, J.B., Kahmen, A., 2012. Molecular paleohydrology: interpreting the hydrogen- isotopic composition of lipid biomarkers from photosynthesizing organisms. Annu. Rev. Earth Planet. Sci. 40 (40), 221–249.

Sachse, D., Gleixner, G., Wilkes, H., Kahmen, A., 2010. Leaf wax *n*-alkane δD values of field-grown barley reflect leaf water δD values at the time of leaf formation. Geochim. Cosmochim. Acta 74, 6741–6750.

Sachse, D., Kahmen, A., Gleixner, G., 2009. Significant seasonal variation in the hydrogen isotopic composition of leaf-wax lipids for two deciduous tree ecosystems (Fagus sylvativa and *Acer pseudoplatanus*). Org. Geochem. 40, 732–742.

Sachse, D., Radke, J., Gleixner, G., 2006. Delta D values of individual *n*-alkanes from terrestrial plants along a climatic gradient — implications for the sedimentary biomarker record. Org. Geochem. 37, 469–483.

Schimmelmann, A., Sessions, A.L., Mastalerz, M., 2006. Hydrogen isotopic (D/H) composition of organic matter during diagenesis and thermal maturation. Annu. Rev. Earth Planet. Sci. 34, 501–533.

Schmitz, B., Pujalte, V., 2003. Sea-level, humidity, and land-erosion records across the initial Eocene thermal maximum from a continental-marine transect in northern Spain. Geology 31, 689–692.

Schmitz, B., Pujalte, V., 2007. Abrupt increase in seasonal extreme precipitation at the Paleocene-Eocene boundary. Geology 35, 215–218.

Secord, R., Bloch, J.I., Chester, S.G.B., Boyer, D.M., Wood, A.R., Wing, S.L., Kraus, M.J., McInerney, F.A., Krigbaum, J., 2012. Evolution of the earliest horses driven by climate change in the Paleocene-Eocene Thermal Maximum. Science 335, 959–962.

Secord, R., Wing, S.L., Chew, A., 2008. Stable isotopes in early Eocene mammals as indicators of forest canopy structure and resource partitioning. Paleobiology 34, 282–300.

Sessions, A.L., Burgoyne, T.W., Hayes, J.M., 2001. Determination of the H-3 factor in hydrogen isotope ratio monitoring mass spectrometry. Anal. Chem. 73, 200–207.

Sessions, A.L., Sylva, S.P., Summons, R.E., Hayes, J.M., 2004. Isotopic exchange of carbon-bound hydrogen over geologic timescales. Geochim. Cosmochim. Acta 68, 1545–1559.

Sharp, Z., 2007. Principles of Stable Isotope Geochemistry. Pearson Education, Upper Saddle River, NJ .

Simons, E.L., 1960. The Paleocene Pantodonta. Trans. Am. Philos. Soc. 50, 1–99.

Sluijs, A., Bowen, G.J., Brinkhuis, H., Lourens, L.J., Thomas, E., 2007. The Palaeocene-Eocene Thermal Maximum super greenhouse: biotic and geochemical signatures, age models and mechanisms of global change. In: Williams, M., Haywood, A.M., Gregory, F.J., Schmidt, D.N. (Eds.), Deep-Time Perspectives on Climate Change: Marrying the Signal from Computer Models and Biological Proxies. The Micropalaeontological Society, Special Publications. The Geological Society, London, pp. 323–349.

Smith, F.A., Freeman, K.H., 2006. Influence of physiology and climate on delta D of leaf wax *n*-alkanes from C-3 and C-4 grasses. Geochim. Cosmochim. Acta 70, 1172–1187.

Smith, F.A., Wing, S.L., Freeman, K.H., 2007. Magnitude of the carbon isotope excursion at the Paleocene-Eocene Thermal Maximum: the role of plant community change. Earth Planet. Sci. Lett. 262, 50–65.
Solomon, S., Plattner, G.K., Knutti, R., Friedlingstein, P., 2009. Irreversible climate change due to carbon dioxide emissions. Proc. Natl. Acad. Sci. U. S. A. 106, 1704–1709.
Tipple, B.J., Berke, M.A., Doman, C.E., Khachaturyan, S., Ehleringer, J.R., 2013. Leaf-wax *n*-alkanes record the plant-water environment at leaf flush. Proc. Natl. Acad. Sci. U. S. A. 110, 2659–2664.
Tipple, B.J., Pagani, M., Krishnan, S., Dirghangi, S.S., Galeotti, S., Agnini, C., Giusberti, L., Rio, D., 2011. Coupled high-resolution marine and terrestrial records of carbon and hydrologic cycles variations during the Paleocene-Eocene Thermal Maximum (PETM). Earth Planet. Sci. Lett. 311, 82–92.
Uhen, M.D., Gingerich, P.D., 1995. Evolution of Coryphodon (Mammalia, Pantodonta) in the late Paleocene and early Eocene of northwestern Wyoming. Contributions from the Museum of Paleontology, University of Michigan. 29, pp. 259–289.
Wing, S.L., 1998. Late Paleocene-Early Eocene Floral and Climatic Change in the Bighorn Basin, Wyoming. In: Aubry, M.P., Lucas, S., Berggren, W.A. (Eds.), Late Paleocene-Early Eocene Climatic and Biotic Events in the Marine and Terrestrial Records. Columbia University Press, New York, pp. 380–400.
Wing, S.L., Bloch, J.I., Bowen, G.J., Boyer, D.M., Chester, S., Diefendorf, A.F., Harrington, G.J., Kraus, M.J., Secord, R., McInerney, F.A., 2009. Coordinated sedimentary and biotic change during the Paleocene-Eocene Thermal Maximum in the Bighorn Basin, Wyoming, USA. In: Crouch, E.M., Strong, C.P., Hollis, C.J. (Eds.), Climatic and Biotic Events of the Paleogene (CBEP 2009), Extended Abstracts from an International Conference in Wellington, New Zealand. GNS Science Miscellaneous Series 18, pp. 156–162.
Wing, S.L., Currano, E.D., 2013. Plant response to a global greenhouse event 56 million years ago. Am. J. Bot. 100, 1234–1254.
Wing, S.L., Harrington, G.J., Smith, F.A., Bloch, J.I., Boyer, D.M., Freeman, K.H., 2005. Transient floral change and rapid global warming at the Paleocene-Eocene boundary. Science 310, 993–996.
Winguth, A., Shellito, C., Shields, C., Winguth, C., 2010. Climate response at the Paleocene–Eocene Thermal Maximum to greenhouse gas forcing—a model study with CCSM3. J. Clim. 23, 2562–2584.
Zachos, J.C., Lohmann, K.C., Walker, J.C.G., Wise, S.W., 1993. Abrupt climate change and transient climates during the Paleogene: a marine perspective. J. Geol. 101, 191–213.
Zachos, J.C., Pagani, M., Sloan, L., Thomas, E., Billups, K., 2001. Trends, rhythms, and aberrations in global climate 65 Ma to present. Science 292, 686–693.